Catalysis Science & Technology

PAPER

View Article Online
View Journal | View Issue

Cite this: *Catal. Sci. Technol.*, 2016, **6**, 6057

Perovskites and metal nitrides as catalysts in the base-catalysed aldol addition of isobutyraldehyde to formaldehyde†

Henrike Kleineberg,[a] Matthias Eisenacher,[bc] Horst Lange,[b] Heinz Strutz[b] and Regina Palkovits*[a]

Received 4th September 2015,
Accepted 24th April 2016

DOI: 10.1039/c5cy01479d

www.rsc.org/catalysis

Hydroxypivaldehyde represents an important intermediate in the production of neopentyl glycol, which in turn is widely applied in the production of *e.g.* polyesters, plasticizers, synthetic resin paints and lubricants. It is industrially produced *via* aldol addition of isobutyraldehyde to formaldehyde catalysed by homogeneous bases. However, the major disadvantages include the difficult separation of the base from the product stream, the formation of salts upon neutralisation and side reactions as well as the catalyst's hazard potential due to corrosion, toxicity and inflammability. A set of perovskites and metal nitrides were investigated as solid catalysts for aldol reactions establishing structure–performance correlations. For perovskites, a correlation of the catalytic activity and the degree of distortion as well as the presence of other phases is found but the most promising catalyst, $BaZrO_3$, shows deactivation in recycling experiments. Amongst the metal nitrides, AlN exhibits high activity and stability in batch recycling experiments. Transferring the system into a continuous fixed bed reactor reveals high stability over 150 h time on stream at 423 K. XRD and SEM/EDX confirm the formation of boehmite caused by the hydrolysis of AlN in an aqueous reaction medium. This transformation is associated with a significant increase in the basicity and acidity of the material, which is proposed to account for its high catalytic activity.

Introduction

Heterogeneous catalysis plays an important role in a great number of chemical production processes with major focus on solid acids due to their great importance in petrochemistry.[1] Solid base catalysts have attracted less attention, although their application in many base-catalysed industrial processes offers opportunities to facilitate separation, achieve a higher purity of the product and avoid corrosion problems and waste generation.[2]

A base-catalysed reaction of great industrial importance is the aldol addition of isobutyraldehyde (iBa) to formaldehyde (FA) producing hydroxypivaldehyde (HPA) (Scheme 1). HPA is an intermediate in the production of neopentyl glycol (NPG), which in turn is widely applied in the production of *e.g.* polyesters, plasticizers, synthetic resin paints and lubricants.[3] Traditionally, the aldol addition of iBa to FA is catalysed by homogeneous bases such as alkaline metal hydroxides or trialkylamines.[4–8] Therewith, yields of HPA of up to 87% are achieved.[5] However, these catalysts exhibit a number of disadvantages, which are related to the elaborate separation from the product stream, the formation of salts upon neutralisation and side reactions as well as the catalyst's hazard potential due to corrosion, toxicity and inflammability.[9–16] It is therefore desirable to establish a solid base catalyst for the heterogeneously catalysed aldol addition of iBa to FA. To this point, only a limited number of solid catalysts have been investigated in the described aldol addition. Amongst them are basic ion exchange resins,[16,17] hydrated magnesium oxide[18] as well as base-modified clays.[13]

Two material classes, which have not received much attention as solid base catalysts, are perovskites and metal nitrides. Perovskites are described by the general formula ABO_3, with cation A being of larger size than cation B.[19] In the perovskite structure, the A cation is located in the centre of the cubic unit cell and coordinated to 12 oxygen anions.[20]

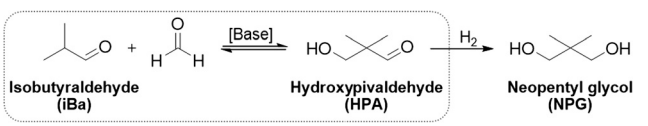

Scheme 1 Base-catalysed aldol addition of iBa to FA followed by hydrogenation to produce NPG.

[a] *Institut für Technische und Makromolekulare Chemie, RWTH Aachen University, Worringerweg 2, 52074 Aachen, Germany. E-mail: palkovits@itmc.rwth-aachen.de*
[b] *OXEA GmbH, Otto-Roelen-Strasse 3, 46147 Oberhausen, Germany*
[c] *TH Köln University of Applied Sciences, CHEMPARK Leverkusen, Kaiser-Wilhelm-Allee, 51368 Leverkusen, Germany*

† Electronic supplementary information (ESI) available. See DOI: 10.1039/c5cy01479d

The B cation is found at the corners of the cubic unit cell and is 6-fold coordinated with oxygen anions. An ideal perovskite structure is formed if the ionic radii of the involved cations and anions yield a tolerance factor t of 1 according to the equation: $t = (r_A + r_O)/\sqrt{2}(r_B + r_O)$.[19] With deviating tolerance factor, the structure becomes increasingly distorted and at $t < 0.8$, the perovskite structure is no longer formed.[20,21] To the best of our knowledge, the only application of perovskites as catalysts for aldol reactions to this point was reported by Torres-Martínez *et al.*[22] They catalysed the gas phase aldol condensation of acetone by alkali tantalates ($ATaO_3$, with A = Li, Na and K). With respect to metal nitrides, Bej *et al.*[23] reported the application of molybdenum nitride as a catalyst in the gas phase aldol condensation of acetone. Hasni *et al.*[24,25] discussed the oxynitride-catalysed aldol condensation of cyclopentanone with valeraldehyde and heptanal with benzaldehyde, respectively.

Herein, we present the potential of perovskites and metal nitrides as solid bases, evaluating their catalytic performance in aldol addition of iBa to FA. The investigated perovskites include the material series A = Ca, Sr and Ba, and B = Ti, Zr and Ce. Amongst the metal nitrides, aluminium nitride, silicon nitride, titanium nitride, titanium carbon nitride as well as tantalum nitride were applied. The materials were characterised, tested in aldol addition and recycled in batch experiments. Additionally, the most promising catalyst was studied in a continuous fixed bed reactor to examine the catalyst stability.

Experimental

Catalyst preparation

The synthesis of perovskites containing titanium as the B cation was performed according to the method described by Li *et al.*[26] In a typical synthesis, 0.87 g (0.011 mol) of titanium oxide (TiO_2, technical, Sigma-Aldrich, ≥99%) were intensively mixed with an equimolar amount of calcium nitrate ($Ca(NO_3)_2{\cdot}xH_2O$, Aldrich, 99.997%), strontium nitrate ($Sr(NO_3)_2$, Sigma-Aldrich, ≥99,0%) or barium nitrate ($Ba(NO_3)_2$, Sigma-Aldrich, ≥99%), respectively. The mixture was calcined at 600 °C for 10 h (heating rate: 4 °C min^{-1}).

The perovskites containing zirconium or cerium as the B cation with A = Ca, Sr or Ba were synthesised by the thermal decomposition of the respective metal nitrate salts. Typically, the particular nitrate salt was thoroughly mixed in an equimolar ratio to produce 2 g of the desired perovskite. The nitrate mixture was calcined at 650 °C for 10 h (heating rate: 2 °C min^{-1}).

The metal nitrides AlN (Grade C and K), Si_3N_4 (Grade M9 (95.7% purity) and M11 (90.8% purity)), TiN (Grade C), Ti(C, N) (Grade C, 50/50) and TaN used in this work were commercial samples obtained from H.C. Starck and were applied without any further pretreatment.

Catalyst characterisation

Powder X-ray diffraction (XRD) patterns were acquired with a D500 Siemens diffractometer using Cu Kα radiation in the 2θ range of 3–90° with an angular step of 0.02°. X-ray fluorescence (XRF) spectroscopy was used to determine the chemical composition of the perovskite samples. Spectra were recorded under vacuum on an Eagle II spectrometer (Röntgenanalytik Systeme). Temperature-programmed desorption (TPD) of CO_2 and NH_3, respectively, were measured on a Quantachrome Instruments ChemBET Pulsar TPD/TPR apparatus with a thermal conductivity detector. Prior to the measurement, the sample was pretreated at 723 K in a helium flow (24 mL min^{-1} in CO_2-TPD and 30 mL min^{-1} in NH_3-TPD, respectively) for 30 min. The adsorption of the probe molecules occurred at 298 K for 30 min in a flow of CO_2 (99.995%, 24 mL min^{-1}) or NH_3 (50% in argon, 30 mL min^{-1}), respectively. The weakly adsorbed probe gas was removed by flushing the measurement cell with helium for another 30 min. The TPD measurement was carried out by ramping in helium with 20 K min^{-1} to 973 K. Scanning electron microscopy with energy dispersive X-ray spectroscopy (SEM/EDX) was performed by the Central Facility for Electron Microscopy (GFE) of RWTH Aachen University. The sample powder was fixed in liquid conductive silver and polished by a cross section polisher. Diffuse reflectance infrared Fourier transform spectra (DRIFTS) were measured on a Bruker VERTEX 70 spectrometer, equipped with a Praying Mantis Diffuse Reflection Accessory and a high temperature reaction chamber (Harrick). Before the measurement, the sample was pretreated at 723 K for 30 min in a nitrogen stream. The spectra were recorded at 303 K in a nitrogen stream (24 mL min^{-1} after CO_2 adsorption and 55 mL min^{-1} after pyridine adsorption, respectively), collecting 512 scans with a resolution of 4 cm^{-1} in the wavenumber range of 4000–850 cm^{-1}. The spectrum of the pretreated sample before probe gas adsorption was used as the respective background spectrum. Thermogravimetric analyses (TGA) were conducted on a Netzsch STA 409 device.

Catalytic experiments

Autoclave experiments. Batch experiments of the aldol addition of iBa to FA were carried out in a Berghof DAB-2 pressure autoclave with a 50 mL PTFE inlet. 12 mL (0.13 mol) of iBa and 9 mL (0.12 mol) of FA solution (aqueous, 37%) were reacted with 5 wt% catalyst for 90 min at 423 K under argon atmosphere and rigorous stirring. After cooling down the reaction mixture to room temperature, the catalyst was separated by centrifugation and the biphasic product solution was homogenised by addition of isopropanol. The resulting solution was analysed by gas chromatography (GC), using a flame ionisation detector (FID) and a 30 m Agilent DBWax column.

Catalyst recycling. In order to investigate the recyclability of the chosen catalysts, the aldol addition was first carried out under standard conditions. After the reaction was finished, the catalyst was separated from the product solution, washed with 100 mL of distilled water and 75 mL of isopropanol and subsequently dried at 100 °C for 20 h. The catalyst was then re-calcined under the conditions applied during synthesis. The regenerated catalyst was applied again in the

aldol addition, adjusting the substrate amounts when needed so as to retain the original catalyst to substrate ratio.

Continuous reaction. The continuous aldol reaction of iBa with FA was conducted in a fixed bed reactor setup. The substrate solution was pumped into the reactor by an HPLC pump, applying a constant flow rate of 0.025 mL min^{-1}. The fixed bed reactor was positioned in an oven to adjust the reaction temperature. The pressure within the setup was controlled by a pressure regulation unit, allowing a constant pressure of 30 bar with consistent flow rate. The substrate solution used contained iBa and FA in a ratio of 1 : 1 and 16 vol% isopropanol with respect to the volume of substrates to obtain a single-phase solution. The catalyst bed consisted of 2.85 g of the 63–90 μm particle size fraction. The contact time at a flow rate of 0.025 mL min^{-1} averaged 108 min. Samples of the product solution were taken at defined time intervals, diluted in isopropanol and analysed by GC according to the description above.

Results and discussion

3.1. Catalyst characterisation

The synthesised perovskite catalysts as well as the commercial metal nitrides all together exhibited specific surface areas that were too low to be determined with sufficient accuracy by nitrogen sorption measurements.

The XRD patterns of the synthesised perovskite-type catalysts generally display the typical reflections of the desired compounds (Fig. 1). Besides the typical perovskite reflections, most XRD patterns also show additional reflections of the B oxides, *i.e.* TiO_2, ZrO_2 or CeO_2. This observation can be attributed to non-stoichiometry within the perovskite structure which is commonly known for this class of materials and has been described elsewhere.[19] The B cations form a stable framework which allows A cation vacancies to occur, *e.g.* due to volatilisation at elevated temperatures, without impairing the perovskite structure. The defective perovskite structures can also be observed in the composition of the materials determined by XRF. The perovskite structure requires an A to B cation ratio of 1 : 1. As shown in Table 1, the majority of the determined values for the amount of A and B cations within the respective compounds do not comply with this ratio. However, in most cases it is shifted towards the B cation, meaning that the A cation has only partially been incorporated into the structure or an additional phase of the B cation has been formed.

A special case among the considered perovskites is the Ca and Ce containing material. In contrast to the other XRD patterns, that of the named compound does not show any reflections of the perovskite phase. Instead, the reflections of the coexisting CaO and CeO_2 phases are observed. A glance at the calculated tolerance factor for this compound (Table 2) explains this fact, as tolerance factors of $t < 0.8$ do not permit the formation of the perovskite phase.[21]

As the applied metal nitrides were commercial samples and used without further purification, the phase purity of the samples was validated by XRD measurements. The obtained XRD patterns shown in Fig. 2 confirm the presence of the respective metal nitride phases in all cases. The XRD patterns of Si_3N_4 and TaN additionally exhibit some small reflections besides the nitride phase which can be attributed to impurities and TaC, respectively.

Table 1 Composition of the synthesised perovskite-type catalysts, determined by XRF

Perovskite ABO_3	*n*(cation A) [mol%]	*n*(cation B) [mol%]
$CaTiO_3$	43.2	56.8
$SrTiO_3$	57.2	42.8
$BaTiO_3$	28.9	71.1
$CaZrO_3$	34.0	66.0
$SrZrO_3$	50.0	50.0
$BaZrO_3$	43.0	57.0
$CaCeO_3$[a]	—	—
$SrCeO_3$	41.8	58.2
$BaCeO_3$	38.9	61.1

[a] No sufficient material available for analysis.

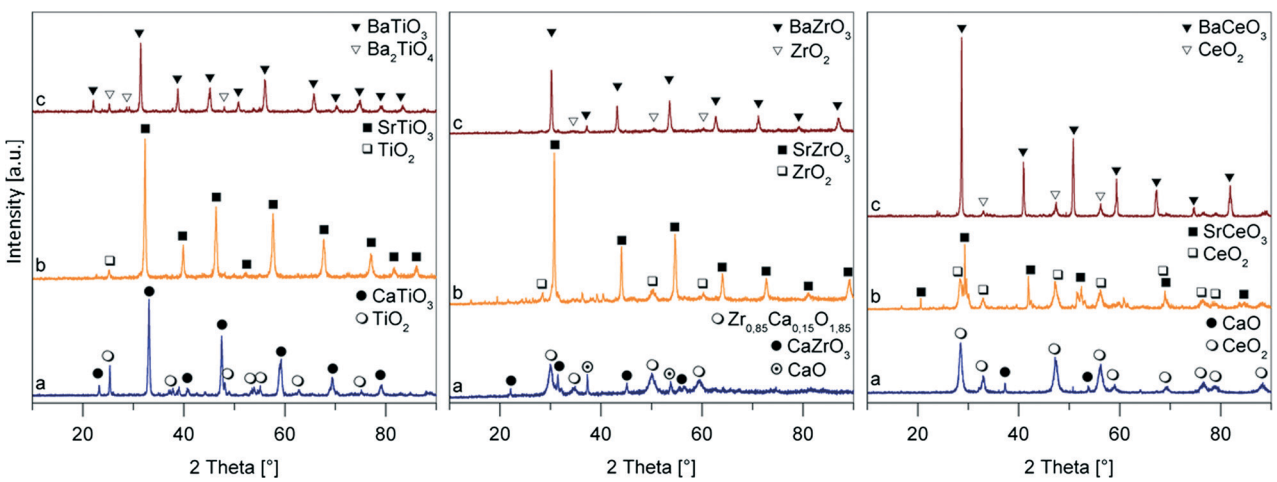

Fig. 1 XRD patterns of the synthesised perovskite-type catalysts.

Table 2 Ionic radii and tolerance factors of the synthesised perovskite-type catalysts

Perovskite ABO_3	Ionic radius [Å][a,b] Cation A		Cation B		Tolerance factor[c]
$CaTiO_3$	Ca^{2+} (VIII)	1.12	Ti^{4+} (VI)	0.605	0.89
$SrTiO_3$	Sr^{2+} (XII)	1.44	Ti^{4+} (VI)	0.605	1.00
$BaTiO_3$	Ba^{2+} (XII)	1.61	Ti^{4+} (VI)	0.605	1.06
$CaZrO_3$	Ca^{2+} (VIII)	1.12	Zr^{4+} (VI)	0.72	0.84
$SrZrO_3$	Sr^{2+} (XII)	1.44	Zr^{4+} (VI)	0.72	0.95
$BaZrO_3$	Ba^{2+} (XII)	1.61	Zr^{4+} (VI)	0.72	1.00
$CaCeO_3$	Ca^{2+} (VIII)	1.12	Ce^{4+} (VI)	0.87	0.78
$SrCeO_3$	Sr^{2+} (XII)	1.44	Ce^{4+} (VI)	0.87	0.88
$BaCeO_3$	Ba^{2+} (XII)	1.61	Ce^{4+} (VI)	0.87	0.94

[a] Data from ref. 27. [b] Numbers in parentheses describe the coordination of the ion within the perovskite. [c] Ionic radius of O^{2-} (VI): 1.40 Å.

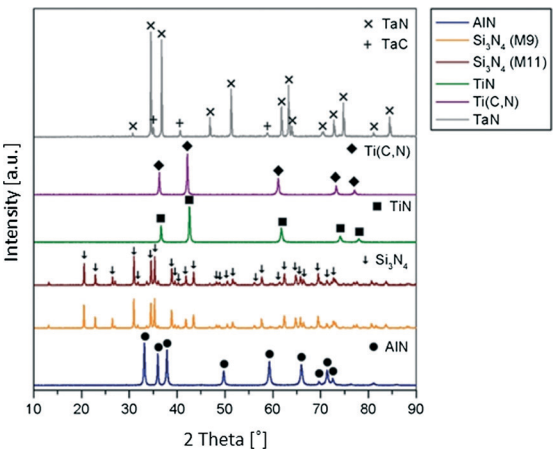

Fig. 2 XRD patterns of metal nitride catalysts.

3.2. Catalyst screening

Regardless of the actual crystal phase observed by XRD, all synthesised perovskite-type materials were applied in the batch aldol addition of iBa to FA. The obtained catalytic results are presented in Fig. 3. The highest yields of the desired product are obtained using $SrZrO_3$ or $BaZrO_3$ as a catalyst, producing 53% HPA at an iBa conversion of 91%. Within the group of compounds containing Ti as the B cation, the conversion of iBa appears to correlate with the tolerance factor of the perovskites (Table 2). As the tolerance factor is a measure for the ideality or distortion of the cubic perovskite structure, the activity of the perovskites can be related to the degree of their distortion. This observation was also made by Torres-Martínez *et al.*[22] who applied alkali tantalates in the gas phase aldol reaction of acetone. They found that the most distorted $LiTaO_3$ showed the highest basicity and activity in the reaction. In contrast, the opposite trend occurs for Zr and Ce as B cations exhibiting increasing catalytic activity for a tolerance factor of approximately 1. In line with this, a possible explanation could be related to the potential contribution of the other phases existing in the material besides the perovskite phase. Indeed, reference experiments with ZrO_2 and CeO_2 revealed 44 and 37% iBa conversion, respectively. However, considering their low amount in the samples, a major contribution to the catalytic activity appears unlikely.

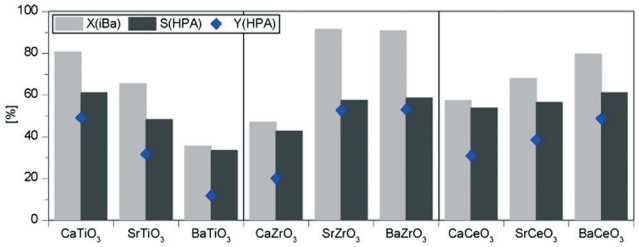

Fig. 3 Catalytic results of the perovskite-type materials in the aldol addition of iBa to FA at 423 K for 90 min using 5 wt% of catalyst.

The commercially obtained metal nitride samples were likewise applied in the catalytic aldol addition of iBa to FA. The catalytic results gained from these experiments are depicted in Fig. 4. The catalytic activities of the investigated metal nitrides differ quite strongly from each other. Interestingly, silicon nitride with a higher purity (grade M9) shows a lower conversion of iBa than the material with greater impurities (grade M11). This leads to the assumption that not Si_3N_4 but the impurities represent the active species, or the impurities create some sort of defects in the nitride structure, therefore enhancing the catalytic activity. Comparing the catalytic results of TiN and Ti(C,N), Ti(C,N) exhibits considerably higher conversion of iBa and selectivity towards HPA. Thus, the presence of titanium carbide within the compound has a positive influence on the catalytic activity. The lowest catalytic conversion was obtained using TaN, while AlN showed the highest activity with a conversion of 88% and an HPA yield of 52%.

3.3 Catalyst recycling

Because of its promising catalytic activity, $BaZrO_3$ was found exemplary as a perovskite to investigate its stability and recyclability in the aldol addition of iBa to FA. The gained results for this recycling experiment over three runs are shown in Fig. 5. The conversion of iBa experiences a slight decrease over three reaction runs, while the selectivity towards HPA remains constant. Upon homogenisation with isopropanol, colorless needle-shaped crystals precipitated from the product solution. These were separated, dried and investigated by XRD measurement. Although we were not able to attribute

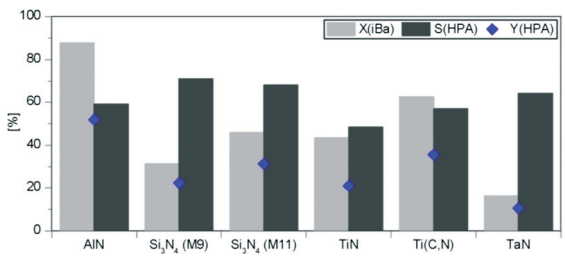

Fig. 4 Catalytic results of the metal nitrides in the aldol addition of iBa to FA at 423 K for 90 min using 5 wt% of catalyst.

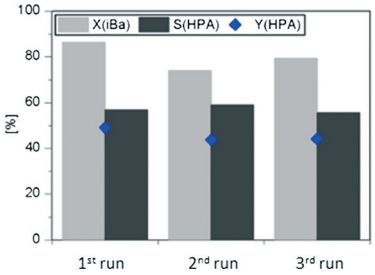

Fig. 5 Recyclability of $BaZrO_3$ in the aldol addition of iBa to FA at 423 K for 90 min using 5 wt% of catalyst.

the obtained reflections to a specific crystal phase, we suggest that the precipitate is some sort of organic compound of barium or zirconium.

This assumption is based on the finding in the same reaction using Zn/Al and Co/Al hydrotalcites as catalysts. Therein, the precipitated crystals could be identified as the formate salts of zinc and cobalt, respectively. Furthermore, comparing the XRD spectra of fresh $BaZrO_3$ and the regenerated catalyst after the third reaction run (Fig. 6), the reflections assigned to ZrO_2 are much more pronounced in the latter. This implies that barium leached from the perovskite structure, leaving a greater amount of ZrO_2 to coexist with the perovskite phase. Thus, the leaching of barium species could be an explanation for the decrease in catalytic activity.

As for the perovskites, AlN was selected for a recycling experiment because of its outstanding catalytic performance among the metal nitrides. The results obtained for three runs are depicted in Fig. 7. As the conversion of iBa and the selectivity towards HPA remain constant in all three reactions, no deactivation of the catalyst could be determined. In order to observe a possible change in the catalyst's structure during recycling, fresh AlN as well as the catalysts after reaction and regeneration were investigated using XRD. Hereby, the regenerated samples are described as AlN-R*x*, with *x* being the regeneration step after the *x*th reaction run. The recorded XRD patterns are shown in Fig. 8. It has to be noted beforehand that only a small sample amount was available for the measurement of AlN-R2, thus the reflections in this XRD pattern are of low intensity. While the XRD of fresh AlN shows

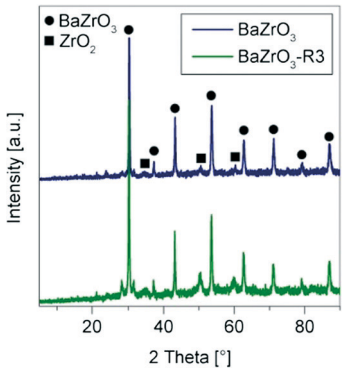

Fig. 6 XRD patterns of fresh $BaZrO_3$ and the regenerated catalyst after the third run ($BaZrO_3$-R3).

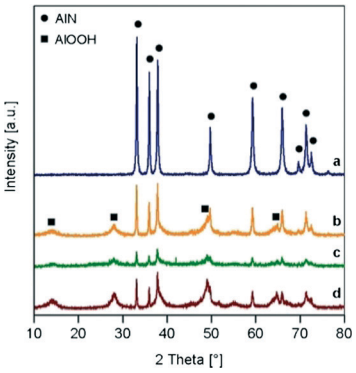

Fig. 7 XRD patterns of (a) fresh AlN and regenerated catalysts after the (b) first, (c) second and (d) third run.

solely the reflections of the AlN phase, the XRD patterns of the three regenerated samples show additional reflections of boehmite (AlOOH). The boehmite phase is generated in the hydrolysis of AlN with water from the aqueous reaction solution. According to the corresponding reaction pathway published by Bowen *et al.*[28] AlN reacts at room temperature with water and under elimination of ammonia to produce amorphous AlOOH. In a basic aqueous reaction medium, the amorphous AlOOH then recrystallizes to give $Al(OH)_3$.

$$AlN + 2H_2O \rightarrow AlOOH_{(amorph.)} + NH_3$$

$$NH_3 + H_2O \rightleftharpoons NH_4^+ + OH^-$$

$$AlOOH_{(amorph.)} + H_2O \xrightarrow{OH^-} Al(OH)_{3(crsytal.)}$$

This model was extended for elevated temperatures by Kocjan *et al.*[29] They suggested that some of the initially formed amorphous AlOOH is dissolved and reprecipitated to form crystalline AlOOH, while some transforms to crystalline $Al(OH)_3$ *via* a dissolution/recrystallization process. It is proposed that $Al(OH)_3$ is formed at low temperatures, high pH values and long hydrolysis times. However, at higher temperatures and moderate pH values boehmite is thermodynamically more stable.

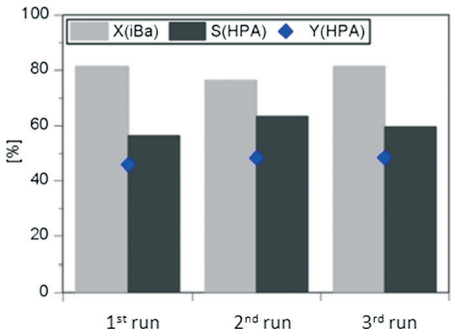

Fig. 8 Recyclability of AlN in the aldol addition of iBa to FA at 423 K for 90 min using 5 wt% of catalyst.

$$AlOOH_{(amorph.)} \rightarrow AlOOH_{(crsytal.)}$$
$$AlOOH_{(amorph.)} + H_2O \rightarrow Al(OH)_{3(crsytal.)}$$

The aldol addition investigated in this work was carried out at 150 °C for 90 min in a relatively large volume of aqueous solution, in which pH variation is expected to be rather low. Regarding the reaction conditions applied, it is obvious why no reflections of $Al(OH)_3$ are observable in the XRD patterns of the regenerated catalyst samples.

The formation of an oxygen-containing phase in aluminum nitride during the reaction was furthermore observed using SEM/EDX measurements. Fig. 9 shows the SEM images of fresh AlN and the regenerated AlN-R3 sample. The streaky appearance of the particles of both materials is due to the polishing procedure during sample preparation. Concerning fresh AlN, only aluminum and nitrogen are detected both in the middle and the marginal area of the particle shown. These observations indicate the presence of pure aluminum nitride. For the AlN-R3 sample, however, additional oxygen, and at the edge of the particle only aluminum and oxygen are detected. This leads to the assumption that the hydrolysis of AlN does not only take place at the surface, but advances inside the particle. The silver signal that appears in the spectrum of AlN-R3 does not actually present part of the sample but results from the conductive silver, which was used for sample fixture.

In order to explain the high catalytic activity of aluminum nitride in the aldol addition of iBa to FA, the basic and acidic properties of the fresh AlN and the already applied catalyst material were investigated using temperature-programmed desorption of CO_2 and NH_3, respectively. Additionally, TaN was examined as its performance in the aldol addition had been proven to be rather low. The obtained TPD spectra of all three materials are depicted in Fig. 10. It shows that for TaN no measurable signals of desorbed CO_2 or NH_3, respectively, were detected which leads to the conclusion that this

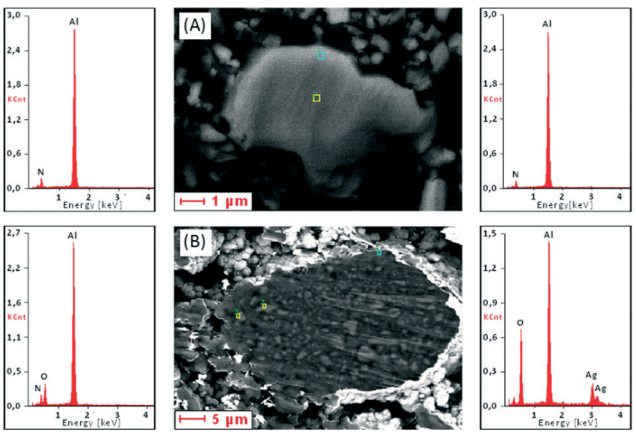

Fig. 9 SEM/EDX results of (A) fresh AlN and (B) the regenerated catalyst after the third run.

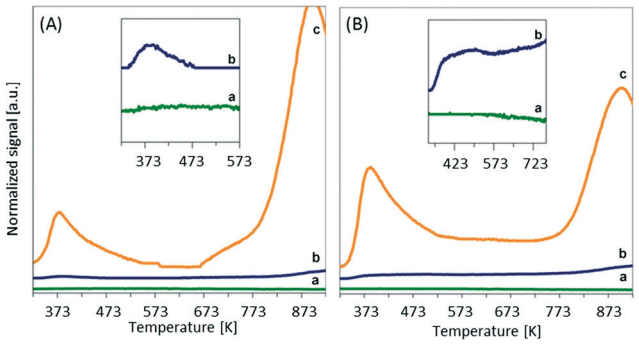

Fig. 10 (A) TPD-CO_2 and (B) TPD-NH_3 spectra of (a) TaN, (b) fresh AlN and (c) regenerated AlN catalyst after the first run (AlN-R1).

nitride itself does not possess any basic or acidic sites. The spectra of fresh AlN show only very weak signals that, according to the desorption temperature at which they occur, can be attributed to mainly weak basic and acidic sites. The origin of these sites is not fully clarified yet but probably related to partial surface hydrolysis. The spectra of AlN-R1, however, reveal significantly stronger signals both in the TPD spectra of CO_2 and NH_3. Corresponding to the strong desorption signal in the TPD-CO_2 spectra at around 378 K, a major part of the basicity arises from the weak basic sites. In the TPD-NH_3 spectra, the most obvious signal is found at 383 K, which can be assigned to weak acid sites. Additionally, spectra deconvolution suggests further contributions at around 443 and 684 K for medium to strong acid sites (Fig. S1, ESI†). The signal at about 903 K which appears both in the TPD-CO_2 and TPD-NH_3 spectra is presumed to be a result of water that is formed during the decomposition of the boehmite phase. Integration of the TPD signals allowed the estimation of the concentration of basic and acidic sites of the respective catalysts. The data are presented in Table 3. The total basicity of fresh AlN increased almost by a factor of 20 in AlN-R1 due to the hydrolysis of AlN and thus the formation of boehmite. About 75% of the basicity can be attributed to the weak basic sites. These occur in the form of Brønsted hydroxyl groups, which in turn are known to be the active species in catalytic aldol reactions.[30–34] Further, the concentration of acidic sites in AlN-R1 is more than an order of magnitude higher than that in fresh AlN. Accordingly, the observed catalytic activity of AlN in the first catalytic run is likely caused by fast surface reconstruction of the material into amorphous AlOOH followed by recrystallization providing an enhanced concentration of the surface basic and acidic sites responsible for the catalytic activity.

Table 3 Basic and acidic characteristics of the metal nitrides

	c(basic sites) [mmol g^{-1}]		*c*(acidic sites) [mmol g^{-1}]	
Catalyst	Total	Weak	Total	Weak
TaN	—	—	—	—
AlN	0.005	0.002	0.079	0.012
AlN-R1	0.093	0.068	0.987	0.208

To determine the nature of the basic and acidic sites on AlN-R1, DRIFT spectroscopy after adsorption of CO_2 or pyridine, respectively, was realized. The recorded spectra are shown in Fig. 11. The spectra after adsorption of CO_2 reveal the distinct signals of bicarbonate species at 1650, 1443, and 1219 cm^{-1}, and unidentate carbonate at 1558–1505 cm^{-1}.[35] These surface species of adsorbed CO_2 are related to the Brønsted basic hydroxyl groups and Lewis basic O^{2-} anions, respectively, which is in accordance with the thermal stability of the carbonates regarding the disappearance of the corresponding signals at elevated temperatures. Two further signals appear at 1593 and 1392 cm^{-1}, which are thought to be related to the weakly bound species due to their disappearance at 373–473 K. The spectra after pyridine adsorption exhibit strong signals at 1591 and 1442 cm^{-1} resulting from hydrogen bridged pyridine.[36,37] This type of adsorbed species is found on Brønsted acidic hydroxyl groups. The signal at 1442 cm^{-1} masks the signal at about 1445 cm^{-1}, becoming visible only at elevated temperatures due to the desorption of hydrogen bridged pyridine, and thus the disappearance of the corresponding signal. Because of the position and thermal stability of the revealed signal, it is suggested to be associated with pyridine coordinated on strong Lewis acidic Al^{3+} cations. At 1490 and 1479 cm^{-1}, two additional signals attributed to the presence of Brønsted and Lewis acidic sites are observed.

The deviation of the results obtained from DRIFT spectroscopy and TPD is found to be due to different thermal treatment procedures, and especially in the characterization of acidic properties, the use of two different probe molecules. In conclusion, the high catalytic activity of AlN-R1 is suggested to be a result of the increased concentration of both basic and acidic sites on the catalyst's surface. This observation is in good accordance with the findings of Hasni *et al.*[24] whose results reveal that amphoteric Al_2O_3 generates higher conversions in the aldol condensation of cyclopentanone with valeraldehyde than strongly basic MgO.

As described above, during hydrolysis of aluminum nitride, ammonia is released, which may lead to an increased concentration of hydroxide ions in an aqueous solution. In order to estimate whether the catalytic activity in the aldol addition of iBa to FA is actually caused by the applied catalyst, or purely an effect of an increased pH due to emitted ammonia, a leaching experiment was carried out. Therefore, the aldol addition was first carried out under standard conditions. The catalyst was removed from the product solution and the reaction continued under equal reaction conditions without any catalyst. The gained results in Fig. 12 show that there is no further increase in conversion observable. Thus, it can be assumed that the hydroxide ions resulting from hydrolysis do not represent the active species in the catalytic aldol addition. Meanwhile, the slight decrease in selectivity towards HPA may be attributed to consecutive reactions of HPA in the second reaction run. An additional reference experiment using a commercially available boehmite (Pural TH 100, Sasol) emphasised its catalytic activity for this reaction, delivering an iBa conversion of 73% compare to 81% for AlN (Fig. 7) under these reaction conditions.

3.4. Continuous reaction

To estimate the durability of a catalyst in aldol addition of iBa to FA, continuous reaction experiments in a fixed bed reactor setup were conducted. The reaction was run for 150 h at reaction temperatures of 423 and 393 K, respectively. Fig. 13 presents the catalytic results obtained for both reaction runs. The initial course of the conversion in both cases shows that a few hours at the beginning of the reaction are required until steady state conditions are reached. The reason for that is the mean residence time of over five hours within the reaction setup is related to the small volumetric flow rate. At 423 K, 81% of iBa are converted to HPA with a selectivity of 70% once the steady state is attained. However, within the first 32 h, both the conversion of iBa and the selectivity to HPA are subject to a slight decrease. At 32 h, a constant selectivity of 64% is observed, and the conversion remains constant at 73% from 120 h, producing an HPA yield of 47%. At a lower reaction temperature of 393 K, the conversion of iBa decreases immediately after the beginning of the reaction, leading to HPA yields of mostly below 30% after a time-on-stream of 24 h. However, in comparison, a much higher selectivity to HPA of 85% is recorded throughout the entire reaction run, caused by a lower degree of consecutive reactions of HPA at lower temperatures.

In order to estimate the strong decrease in conversion of iBa at 393 K, while the conversion remained relatively constant at 423 K, thermogravimetric analyses of the fresh AlN

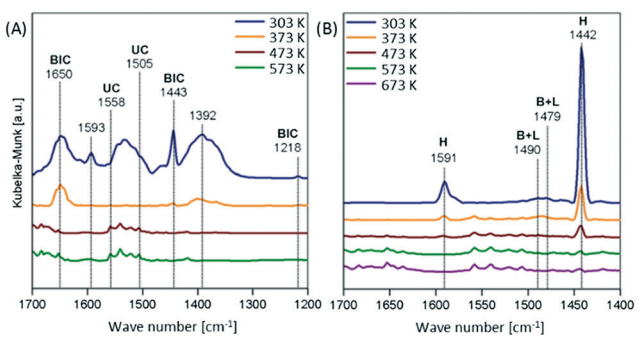

Fig. 11 DRIFT spectra of regenerated AlN after the first run (AlN-R1) after adsorption of (A) CO_2 and (B) pyridine, respectively, and thermal treatment.

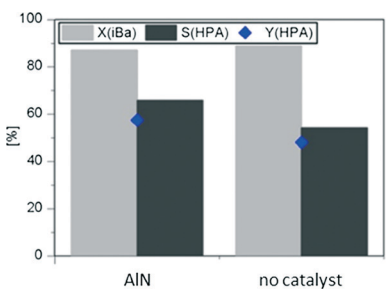

Fig. 12 Leaching experiment of AlN in the aldol addition of iBa to FA at 423 K for 90 min using 5 wt% of catalyst.

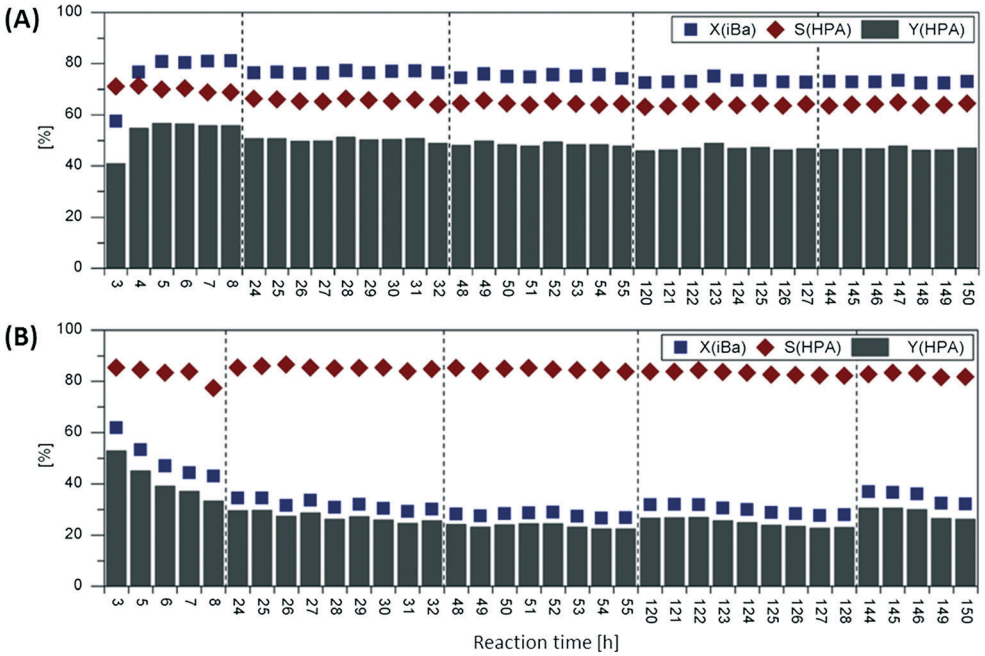

Fig. 13 Continuous aldol reaction of isobutyraldehyde with formaldehyde with AlN as the catalyst at (A) 423 K and (B) 393 K over 150 h.

as well as the used catalysts of both reaction runs were carried out. The recorded TGA curves presented in Fig. 14 show severe differences between the fresh material and the used catalysts. Hence, fresh AlN is stable up to temperatures above 1173 K. The used catalysts, however, undergo two mass losses at 277–523 K and 523–753 K, respectively. As mentioned above, aluminum nitride is hydrolysed to boehmite by water contained in the substrate solution of the aldol addition reaction. Accordingly, the mass loss at 523–753 K can be attributed to the dehydration of AlOOH, forming Al_2O_3. The larger mass loss of the catalyst found in the reaction at 423 K may be explained by a higher content of boehmite, which is formed due to the harsher reaction conditions. The mass loss observed at 277–523 K differs slightly for the catalysts used at 393 and 423 K, respectively. The mass loss is proposed to result from organic compounds, *e.g.* formic acid, which is formed as a typical by-product of aldol addition, adsorbed on the catalyst surface. For the material after reaction at 393 K, the mass loss amounts to 2.2%, while the catalyst applied at 423 K loses only 2.0% of its initial mass. The low catalytic activity of AlN at the temperature of 393 K may therefore be explained by a higher degree of organic species adsorbed on the surface, thus blocking the active sites of the catalyst to a greater extent. As desorption is an endothermic process, the amount of adsorbed species is lower at a higher reaction temperature, allowing for a higher catalytic activity.

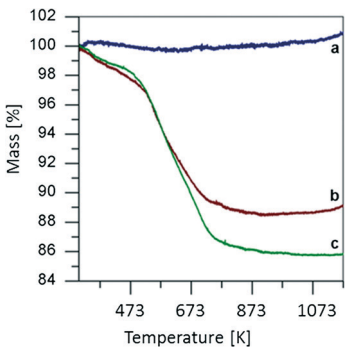

Fig. 14 TGA of (a) fresh AlN and the applied catalyst in the continuous aldol addition of iBa to FA at (b) 393 K and (c) 423 K, respectively.

Conclusions

Different perovskites and metal nitrides were applied as heterogeneous base catalysts in aldol addition of iBa to FA. The catalysts were first tested in batch experiments. Within the group of compounds containing Ti as the B cation, the conversion of iBa appears to correlate with the tolerance factor of the perovskites. The opposite trend becomes apparent for Zr and Ce as B cations, which is potentially related to the contribution of the other phases in the materials to the catalytic activity. $BaZrO_3$ as an exemplary compound of its class lost activity upon recycling, which could be attributed to the leaching of barium from the perovskite structure. Across the metal nitrides, strong deviations in their catalytic activity occurred. Aluminium nitride proved to be the most active candidate. Recycling tests revealed a constant activity over three runs. Investigations using XRD and SEM/EDX demonstrated the formation of a boehmite phase due to hydrolysis of AlN with water from the aqueous reaction solution. Results of TPD with CO_2 and NH_3 showed that the basicity as well as the acidity of the material containing boehmite was largely increased in comparison with the fresh aluminum nitride. It can be concluded that these properties are responsible for the high catalytic activity of the material. The stability test of

this catalyst in a continuous fixed bed reactor for 150 h at 423 K revealed stable conversion and selectivity producing the desired product at a yield of 46%. For a decreased reaction temperature of 393 K, the selectivity increased from 70 to 85%. In contrast, the conversion decreased probably due to a higher degree of adsorbed organic species at 393 compared to that at 423 K.

Acknowledgements

We gratefully acknowledge the cooperation with OXEA GmbH as our project partner. Moreover, we would like to thank H.C. Starck for the supply of a range of different metal nitride samples. We thank B. Hermanns for XRF measurements and K.-J. Vaeßen for XRD and TG analyses.

Notes and references

1 H. Hattori, *Chem. Rev.*, 1995, **95**, 537–558.
2 Y. Ono, *J. Catal.*, 2003, **216**, 406–415.
3 H.-J. Arpe, *Industrial Organic Chemistry, 5th Edition*, Wiley-VCH, Weinheim, 2010.
4 H. Müler, Riedel-de Haën Aktiengesellschaft, DE 1020614, 1956.
5 G. Jacobsen, H. Fernholz and D. Freudenberger, Farbwerke Hoechst Ag, DE 1768274A1, 1968.
6 P. Lappe, H. Springer and J. Weber, *Chem.-Ztg.*, 1989, **113**, 293–304.
7 F. Merger, W. Fuchs, S. Winderl and E. Haarer, BASF AG, DE 1957591A1, 1969.
8 N. Breitkopf, W. Höfs, H. Kalbfell, F. Thönnessen, P. Lappe and H. Springer, Ruhrchemie AG, DE 3644675A1, 1986.
9 R. Fischer, R. Rakoczy, F. Rößner, O. Meyer, S. Grieshammer and B. J. Berger, Süd-Chemie AG, DE 102010055399A1, 2010.
10 G. Dämbkes, P. Lappe, F. Thönnessen and H. Springer, Hoechst Aktiengesellschaft, US 5072058A, 1990.
11 D. Kratz, H. Rust, R. Krokoszinski and V. Helf, BASF AG, DE 19948112A1, 1999.
12 B. Cornils, *Hydrocarbon Process.*, 1980, **59**, 93–102.
13 R. Culp and W. Beavers, Eastman Chemical Company, WO 0000456A1, 1999.
14 D. Pankaj and B. G. Sampat, *Chem. Wkly.*, 2008, 201–204.
15 M. Steiniger, M. Guixa Guardia and K. Stehmeier, BASF SE, WO 2011141470A1, 2011.
16 E. Paatero, E. Nummi, L. P. Lindfors, H. Nousiainen, J. Hietala, L. Lahtinen and R. Haakana, Neste Oy, WO 9829374A1, 1997.
17 M. A. Tike, A. M. Gharde and V. V. Mahajani, *Asia-Pac. J. Chem. Eng.*, 2008, **3**, 333–346.
18 T. Kwok and W. Watkins, Eastman Chemical Company, WO 9735825A1, 1997.
19 M. A. Peña and J. L. G. Fierro, *Chem. Rev.*, 2001, **101**, 1981–2018.
20 M. Misono, *Heterogeneous Catalysis of Mixed Oxides - Perovskite and Heteropoly Catalysts*, Elsevier, Oxford, 2013.
21 J. Twu and P. K. Gallagher, Preparation of Bulk and Supported Perovskites, *In: Properties and Applications of Perovskite-Type Oxides*, ed. L. G. Tejuca and J. L. G. Fierro (Hrsg.), Marcel Dekker, New York, 1993.
22 L. M. Torres-Martínez, M. E. Meza-de la Rosa, L. L. Garza-Tovar, I. Juárez-Ramírez, F. Tzompantzi, G. Del Angel, J. M. Padilla and R. Gómez, *Adv. Mater. Res.*, 2010, **132**, 61–67.
23 S. K. Bej and L. T. Thompson, *Appl. Catal., A*, 2004, **264**, 141–150.
24 M. Hasni, G. Prado, J. Rouchaud, P. Grange, M. Devillers and S. Delsarte, *J. Mol. Catal. A: Chem.*, 2006, **247**, 116–123.
25 M. Hasni, J. Rouchaud, P. Grande, M. Devillers and S. Delsarte, *Mater. Sci. Forum*, 2007, **554**, 37–42.
26 J. Li, Y. C. Zhang, T. X. Wang and M. Zhang, *Mater. Lett.*, 2011, **65**, 1556–1558.
27 R. D. Shannon, *Acta Crystallogr., Sect. A: Cryst. Phys., Diffr., Theor. Gen. Crystallogr.*, 1976, **32**, 751–767.
28 P. Bowen, J. G. Highfield, A. Mocellin and T. A. Ring, *J. Am. Ceram. Soc.*, 1990, **73**, 724–728.
29 A. Kocjan, K. Krnel and T. Kosmač, *J. Eur. Ceram. Soc.*, 2008, **28**, 1003–1008.
30 V. K. Díez, C. A. Ferretti, P. A. Torresi, C. R. Apesteguía and J. I. Di Cosimo, *Catal. Today*, 2011, **173**, 21–27.
31 S. Abelló, F. Medina, D. Tichit, J. Pérez-Ramírez, J. C. Groen, J. E. Sueiras, P. Salagre and Y. Cesteros, *Chem. – Eur. J.*, 2005, **11**, 728–739.
32 M. J. Climent, A. Corma, S. Iborra and A. Velty, *Catal. Lett.*, 2002, **79**, 157–163.
33 K. K. Rao, M. Gravelle, J. Sanchez Valente and F. Figueras, *J. Catal.*, 1998, **173**, 115–121.
34 D. Tichit, M. Naciri Bennani, F. Figueras, R. Tessier and J. Kervennal, *Appl. Clay Sci.*, 1998, **13**, 401–415.
35 J. I. Cosimo, V. K. Díez, M. Xu, E. Iglesia and C. R. Apesteguía, *J. Catal.*, 1998, **178**, 499–510.
36 H. Knözinger, Specific Poisoning and Characterisation of Catalytically Active Oxide Surfaces, *In: Advances in Catalysis*, ed. D. D. Eley, H. Pines and B. W. Paul, Academic Press, 1976, vol. 25.
37 G. Larsen, S. Raghavan, M. Márquez and E. Lotero, *Catal. Lett.*, 1996, **37**, 57–62.